# Masked Auto-Regressive Variational Acceleration: Fast Inference Makes Practical Reinforcement Learning

Yuxuan Gu<sup>1†</sup>, Weimin Bai<sup>1†</sup>, Yifei Wang<sup>2</sup>, Weijian Luo<sup>3</sup>, He Sun<sup>1‡</sup>
1. Peking University 2. Rice University 3. Xiaohongshu Inc

#### **Abstract**

Masked auto-regressive diffusion models (MAR) benefit from the expressive modeling ability of diffusion models and the flexibility of masked auto-regressive ordering. However, vanilla MAR suffers from slow inference due to its hierarchical inference mechanism: an outer AR unmasking loop and an inner diffusion denoising chain. Such decoupled structure not only harm the generation efficiency but also hinder the practical use of MAR for reinforcement learning (RL), an increasingly critical paradigm for generative model post-training. To address this fundamental issue, we introduce MARVAL (Masked Auto-regressive Variational Acceleration), a distillation-based framework that compresses the diffusion chain into a single AR generation step while preserving the flexible auto-regressive unmasking order. Such a distillation with MARVAL not only yields substantial inference acceleration but, crucially, makes RL post-training with verifiable rewards practical, resulting in scalable yet human-preferred fast generative models. Our contributions are twofold: (1) a novel score-based variational objective for distilling masked auto-regressive diffusion models into a single generation step without sacrificing sample quality; and (2) an efficient RL framework for masked auto-regressive models via MARVAL-RL. On ImageNet 256×256, MARVAL-Huge achieves an FID of 2.00 with more than 30 times speedup compared with MARdiffusion, and MARVAL-RL yields consistent improvements in CLIP and image-reward scores on ImageNet datasets with entity names. In conclusion, MARVAL demonstrates the first practical path to distillation and RL of masked autoregressive diffusion models, enabling fast sampling and better preference alignments.

# 1. Introduction

Auto-regressive (AR) [42, 43, 55–57] and diffusion-based [8, 52] generative models exhibit complementary

strengths and weaknesses. Diffusion models excel at high-fidelity synthesis and mode coverage, but require long denoising trajectories with hundreds of iterative updates [17, 46, 49], making inference and downstream Reinforcement Learning (RL) post-training computationally expensive. In contrast, AR models generate sequentially in discrete space, offering natural support for semantic controllability and compatibility with RL and language-based alignment frameworks [9, 35, 41], but they often struggle to match the perceptual quality of state-of-the-art diffusion models at high resolutions. Motivated by their complementary properties, recent works have combined the two paradigms—forming AR+Diffusion [12, 19, 26] architectures that use AR priors to capture global structure and diffusion decoders to restore fine-grained details. The Masked Auto-regressive (MAR) model [26] represents a prominent example of this hybrid design.

However, MAR models face two fundamental limitations. First, their nested architecture—where each AR iteration contains a full diffusion unmasking process—results in extremely slow inference. Second, this inefficiency significantly hinders practices to perform RL-based post-training, which is essential for scalable generative models to be aligned with human preferences[4, 37, 54]. The above two issues encourage us to answer a fundamental research question: Can we improve the efficiency of MAR-like models while making RL post-training practical and efficient?

To this end, we propose *MARVAL* (*M*asked *A*uto-*R*egressive *V*ariational *Accel*eration), which introduces a novel score-based variational distillation principle that compresses the costly diffusion chain into a single masked-AR generation step, preserving the original AR ordering while achieving more than 30× speed-up. Building upon this acceleration, we further develop MARVAL-RL, an RL fine-tuning algorithm that incorporates reward feedback to enhance fidelity and preference alignment.

Empirically, MARVAL-H achieves competitive ImageNet [7]  $256 \times 256$  generation quality (FID = 2.00), which slightly outperforms MAR-H (FID = 2.06) while being  $20 \times$ 

<sup>†</sup>Equal Contributions. ‡Corresponding author.

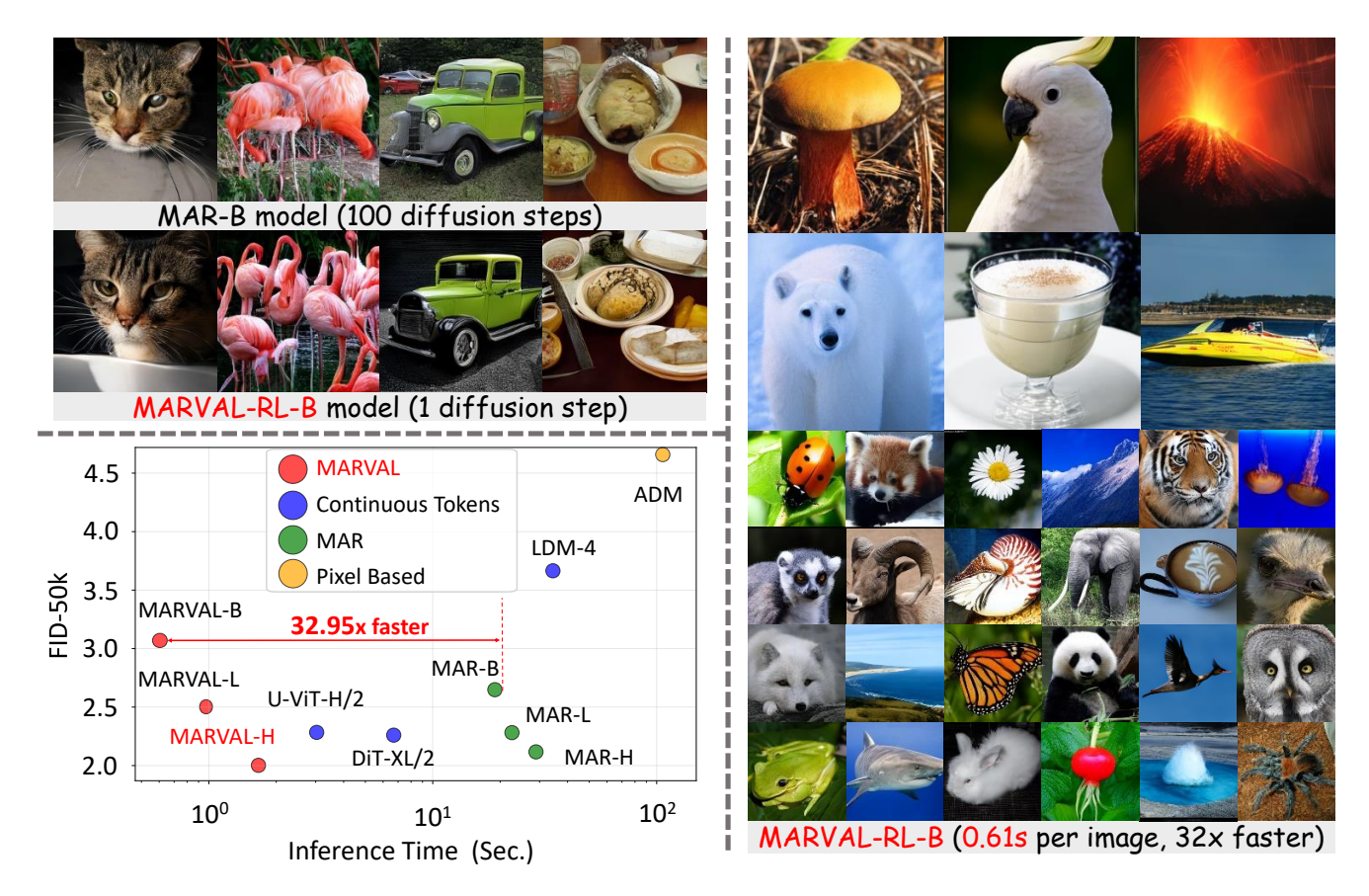


Figure 1. Performance and qualitative results of MARVAL-RL. **Top-left:** Comparison of image quality between the MAR-B model (100 diffusion steps) and the MARVAL-RL-B model (1 diffusion step). MARVAL-RL significantly surpasses the MAR-B model in semantic quality, fidelity, and clarity. **Bottom-left:** Comparing FID-50k (y-axis) and inference time generating one image(x-axis) against other state-of-the-art methods. The MARVAL series (red dots) demonstrates superior performance, achieving low FID scores with significantly faster inference speeds (e.g., MARVAL-H achieves a FID of 2.00, and MARVAL-B is 32.95x faster than MAR-B). **Right:** A collection of diverse, high-quality images generated by MARVAL-RL-B model, showcasing its strong generative capabilities at an average speed of only 0.61 seconds per image.

faster. When post-trained with RL using human preference rewards, MARVAL-RL further improves CLIP and Image Reward scores, demonstrating better alignment with human preferences. As illustrated in Fig. 1, MARVAL-RL delivers visually sharper and semantically richer generations than the MAR baseline while maintaining real-time inference efficiency ( $\approx 0.6~\text{s}$  per image). Together, these results establish MARVAL as a practical and scalable path toward efficient, RL-ready image generative modeling with a masked auto-regressive generation order.

# 2. Related Works

#### 2.1. Diffusion Models

Diffusion models [17, 49, 52] try to train a neural network to model data distribution by gradually corrupting samples with a Gaussian forward diffusion process. From a continuous-time perspective, Song *et al.* [52] general-

ized diffusion models using stochastic differential equations (SDEs). The forward perturbation process is an Itô SDE:

$$dx = f(x_t, t) dt + g(t) dw, \tag{1}$$

where f(x,t) controls the drift and g(t) scales the Brownian motion w at time t. Sampling requires solving the corresponding reverse-time SDE:

$$d\mathbf{x}_t = \left[ f(\mathbf{x}_t, t) - g(t)^2 \nabla_{\mathbf{x}_t} \log p_t(\mathbf{x}_t) \right] dt + g(t) d\overline{\mathbf{w}}, (2)$$

which explicitly involves the score function  $\nabla_{x_t} \log p_t(x_t)$ . Since this quantity is unknown, it is approximated by a neural network  $S_{\theta}(x_t, t)$  by minimizing a weighted denoising score matching loss [51]:

$$\mathcal{L}(\theta) = \mathbb{E}_{t, \boldsymbol{x}_t} \left[ \lambda(t) \| \boldsymbol{S}_{\theta}(\boldsymbol{x}_t, t) - \nabla_{\boldsymbol{x}_t} \log p_t(\boldsymbol{x}_t | \boldsymbol{x}_0) \|_2^2 \right],$$
(3)

where the weighting function  $\lambda(t)$  balances different noise levels. Once trained, the score network can be directly integrated into Eq. 2 to simulate reverse SDEs [20, 52, 64] or ODEs [27, 49], thereby generating high-quality samples.

### 2.2. Masked Auto-regressive Model

The most common practice of traditional diffusion models tries to model the entire image simultaneously in some latent space [22]. However, such a mechanism brings difficulties in modeling complex correlations at potentially high dimensions. Li *et al.* [26] proposed Masked Auto-Regressive Models (MAR), which brings flexible random generation orders by introducing masked auto-regressive ordering. MAR first transforms an image latent representation into n tokens ( $x_1, ..., x_n$ ). Then it randomly masks some tokens in the sequence, and uses the unmasked tokens as conditions to train a lightweight diffusion head to model the denoising process of unmasked tokens.

In inference, MAR uses a bi-level generation pattern: the outer auto-regressive loop controls the gradual unmasking process, which chooses to unmask some more masked tokens, while the inner diffusion chain uses the lightweight diffusion head conditioned on unmasked tokens to generate more tokens from masked ones. In the outer auto-regressive loop unmasking the latent tokens gradually, the *masked auto-regressive* formulation randomly partitions token indices into subsets  $S_1, \ldots, S_K$ , predicting them group by group in K iterations:

$$p(x_1, ..., x_n) = p(S_1, ..., S_K) = \prod_{k=1}^K p(S_k \mid S_{< k})$$

$$S_{< k} = \bigcup_{j < k} S_j,$$
(4)

where  $S_k = \{x_i, x_{i+1}..., x_j\}$  is a set of tokens to be predicted at the k-th step.

The advantage of MAR diffusion is to benefit from the strengths of both sequence modeling and the diffusion models. However, such a bi-level generation pattern brings an unavoidable expensive computation cost, making MAR challenging in real-time generation applications.

## 2.3. One-step Diffusion and Preference Alignment

A major challenge of diffusion models is their slow multistep sampling process, which requires hundreds to thousands of network evaluations. To address this, various distillation techniques have been proposed to accelerate sampling while preserving high-quality generation [2, 11, 13, 21, 25, 28, 30, 36, 45, 47, 48, 50, 53, 60, 61, 63, 66–69]

Score Implicit Matching (SIM) [31] is a recent and powerful approach that enables one-step distillation of a pretrained diffusion model without requiring access to real data

during distillation. Unlike traditional knowledge distillation, which requires a dataset of teacher outputs, SIM operates by directly matching the score functions of the teacher and the student generator. Let the teacher's score function at noise level t be  $s_p(\boldsymbol{x},t)$ , and the generator-induced score be  $s_q(\boldsymbol{x},t)$ . SIM minimizes a time-integrated score divergence between the two:

$$\mathcal{D}_{d} = \int_{0}^{1} \lambda(t) E_{\boldsymbol{x} \sim \pi_{t}} \left[ d(s_{p}(\boldsymbol{x}, t), s_{q}(\boldsymbol{x}, t)) \right] dt, \quad (5)$$

where  $d(\cdot, \cdot)$  is a distance function (e.g., squared distance) and  $\pi_t$  is a reference sampling distribution. A key insight of SIM is that while the generator's score  $s_q$  is intractable, the gradient of this objective with respect to the generator's parameters  $\theta$  can be efficiently computed. This is achieved by training an auxiliary network  $S_{\phi}(x_t, t)$  to approximate  $s_q$ , and then minimizing a tractable surrogate objective derived from the score-divergence gradient theorem [31].

The final training objective for the generator is:

$$\mathcal{L}_{SIM}(\theta) = \int_{t=0}^{T} w(t) \mathbb{E}_{\substack{z \sim p_z, x_0 = g_\theta(z) \\ x_t \mid x_0 \sim q_t(x_t \mid x_0)}} \left[ l(\theta) \right] dt \tag{6}$$

$$l(\theta) = \left\{ -\mathbf{d}'(y_t) \right\}^T \left\{ s_{p_{so[\theta]},t}(x_t) - \nabla_{x_t} \log q_t(x_t \mid x_0) \right\},\,$$

where  $y_t := s_{p_{sg[\theta]},t}(x_t) - s_{q_t}(x_t)$ ,  $g_{\theta}$  is the one-step generator and  $z \sim \mathcal{N}(0,I)$  is pure gaussian noise. The training alternates between updating the generator parameters  $\theta$  using this objective and updating the auxiliary network  $S_{\phi}(x_t,t)$  with a standard denoising score matching loss. This dual-optimization framework allows SIM to effectively distill the knowledge of a multi-step teacher into a single-step generator in a data-free manner.

With the improved techniques of one-step diffusion, several works have explored practices of human preference alignment of diffusion models[3, 5, 6, 10, 18, 24, 39, 40, 59, 65]. Particularly, some recent works [29, 32–34] have advanced the human preference alignment for one-step diffusion models, with rigorous results. However, considering the introduction of random masked auto-regressive ordering, how to properly conduct preference alignment for one-step masked auto-regressive models remains unexplored.

# 3. Method

Our goal is to transform a slow, multi-step auto-regressive generation process, which we refer to as the **teacher**, into a fast, single-step **student** generator to enable the refinement of RL. We achieve this through a unified framework that first distills the conditional generation process in each outer AR loop and then fine-tunes the distilled model to align with human preferences. Our method consists of two main stages: (1) a novel distillation objective, Guided Score Implicit Matching (GSIM), to distill the multi-step pretrained

diffusion denoising network into a single-step generator network  $g_{\theta}$  by predicting the masked tokens from unmasked tokens following MAR's training process, and (2) a reinforcement learning stage that refines  $g_{\theta}$  in the outer autoregressive MAR loop using rewards from designed prompts and generated images. We describe our approach in the context of a Masked Auto-regressive (MAR) model, but the framework is generalizable to any AR+Diffusion architecture with any reward. Figure 2 shows the overall pipeline.

# 3.1. Guided Score Implicit Matching (GSIM)

To overcome the inference latency, our primary contribution is to distill the entire multi-step guided sampling process into a single-step generator,  $g_{\theta}(z,c)$ . Here,  $z \sim p_z$  is a random noise vector sampled from prior distribution  $p_z$ , which is usually designated as the standard gaussian distribution  $\mathcal{N}(0, I)$ . c is the conditional auto-regressive context derived from unmasked tokens. The student generator  $g_{\theta}$  is trained to directly map noise and context to a final, denoised tokens to predict.

While distilling the teacher's multi-step guided sampler into a single-step student generator, we enforce distributional alignment between the student's one-step process and the teacher's multi-step process. We quantify the discrepancy with the KL divergence, leading to the objective:

$$\theta^* := \arg\min_{\theta} \mathbb{E}_{c \sim C} \left[ D_{\text{KL}}(q_{\theta}(\boldsymbol{x}|\boldsymbol{c})||p(\boldsymbol{x}|\boldsymbol{c})) \right], \quad (7)$$

where  $p(\mathbf{x} \mid c)$  is the teacher distribution,  $q_{\theta}(\mathbf{x} \mid c)$  is the student distribution, and  $c \in \mathcal{C}$  denotes the autoregressive context (e.g., class embeddings, unmasked tokens, and mask-position embeddings). However, directly optimizing the objective in Eq. 7 is impossible, because the KL-loss of the two distribution is intractable.

Therefore, we introduce **Guided Score Implicit Match**ing (GSIM). Inspired by the research of Uni-instruct [60], the KL divergence is the integral of the Fisher divergence along a diffusion process under mild regularity conditions. Consequently, Eq. 7 can be expressed in continuous time as the integral over t of the score discrepancy  $D_{\text{score}}$  between the student's time-dependent score  $\nabla_{\mathbf{x}_t} \log q_{\theta,t}(\mathbf{x}_t \mid c)$  and the pretrained diffusion model's score  $s_{p_t}(\mathbf{x}_t, c)$ :

$$\mathcal{D}_{KL}(q_{\theta}(\boldsymbol{x}|\boldsymbol{c})||p(\boldsymbol{x}|\boldsymbol{c})) = \frac{1}{2} \int_{0}^{T} g^{2}(t) \mathbb{E}_{\boldsymbol{x}_{t} \sim q_{\theta, t}} \left[ D_{\text{score}}(\boldsymbol{x}_{t}, \theta) \right] \mathrm{d}t \, \boldsymbol{\theta}^{*} := \arg\min_{\boldsymbol{\theta}} \mathbb{E}_{\substack{\boldsymbol{c} \sim \mathcal{C}, z \sim p_{z}, t \sim \mathcal{U}[0, 1] \\ \boldsymbol{x}_{0} = g_{\theta}(z, c), \ \boldsymbol{x}_{t} \mid \boldsymbol{x}_{0} \sim p_{t}(\boldsymbol{x}_{t} \mid \boldsymbol{x}_{0})}} \left[ L_{GSIM}(\boldsymbol{\theta}) \right],$$

$$D_{\text{score}} = || \underbrace{\nabla_{\boldsymbol{x}_{t}} \log q_{\theta, t}(\boldsymbol{x}_{t} \mid \boldsymbol{c})}_{\text{student score}} - \underbrace{s_{p_{t}}(\boldsymbol{x}_{t}, \boldsymbol{c})}_{\text{teacher score}} ||_{2}^{2},$$

$$L_{GSIM} = L_{1} + L_{2},$$

$$L_{1} = -\left\{ d'\left(y_{t}\right) \right\}^{T} \left\{ s_{q_{\text{sg}[\theta], t}}(\boldsymbol{x}_{t}, \boldsymbol{c}) - \nabla_{\boldsymbol{x}_{t}} \log p_{t}(\boldsymbol{x}_{t} \mid \boldsymbol{x}_{0}, \boldsymbol{c}) \right\}$$

where g(t) is the diffusion coefficient scaling Brownian motion in Eq. 1. The single-step student score  $\nabla_{x_t} \log q_{\theta,t}(x_t \mid$ c) is approximated by an auxiliary network,  $S_{\phi}(x_t, t, c)$ , which is trained on the current set of reconstructions  $x \sim$ 

 $q_{\theta}(x)$  using a standard denoising score matching objective:

$$\mathcal{L}_{auxiliary}(\phi) = \int_{0}^{T} \lambda(t) \mathbb{E}_{\boldsymbol{x}_{t} | \boldsymbol{x}_{0} \sim p_{t}(\boldsymbol{x}_{t} | \boldsymbol{x}_{0})} [l(\phi)] dt,$$

$$l(\phi) = \|\boldsymbol{S}_{\phi}(\mathbf{x}_{t}, t, c) - \nabla_{\mathbf{x}_{t}} \log p_{t}(\mathbf{x}_{t} | \mathbf{x}_{0}, c)\|_{2}^{2}.$$

$$(9)$$

Since MAR employs classifier-free guidance (CFG) [16] during inference, the teacher score  $s_{p_t}(\boldsymbol{x}_t,c)$  in Eq. 8 must correspond to the CFG-guided diffusion process. Accordingly, we define the guided teacher score as:

$$s_{p_t}(\boldsymbol{x}_t, c) = (1+w) \cdot \boldsymbol{S}_p(\boldsymbol{x}_t, t, c) - w \cdot \boldsymbol{S}_p(\boldsymbol{x}_t, t, \emptyset),$$
 (10)

where w is the guidance scale,  $\emptyset$  denotes the null condition, and  $S_p$  is the neural network approximation of the teacher's score. This ensures that the student model learns from the CFG-guided distribution that the teacher actually samples during MAR inference. With all terms in Eq. 8 defined, we now optimize the student parameters  $\theta$  using the following gradient equivalence theorem.

**Theorem** (Gradient Equivalent Theorem). The symbol  $sq[\cdot]$ means stop gradient of some parameters. If distribution  $q_{\theta}(x)$  satisfies some mild regularity conditions, we have the theorem for any score function  $s_{p_{t}}(\cdot)$ :

$$\mathbb{E}_{\boldsymbol{x}_{t} \sim q_{\theta, t}} \frac{\partial}{\partial \theta} d\left(s_{q_{\theta, t}}(\boldsymbol{x}_{t}, c) - s_{p_{t}}(\boldsymbol{x}_{t}, c)\right)$$

$$= \mathbb{E}_{\boldsymbol{x}_{t} \sim q_{\theta, t}} \left[ d'\left(s_{q_{\theta, t}}(\boldsymbol{x}_{t}, c) - s_{p_{t}}(\boldsymbol{x}_{t}, c)\right) \frac{\partial}{\partial \theta} s_{q_{\theta, t}}(\boldsymbol{x}_{t}, c)$$

$$+ \frac{\partial}{\partial \boldsymbol{x}_{t}} d(s_{q_{\theta, t}}(\boldsymbol{x}_{t}, c) - s_{p_{t}}(\boldsymbol{x}_{t}, c)) \frac{\partial \boldsymbol{x}_{t}}{\partial \theta} \right]$$

$$= \frac{\partial}{\partial \theta} \mathbb{E}_{\boldsymbol{x}_{t} \mid \boldsymbol{x}_{0} \sim q_{\theta, 0} \\ \boldsymbol{x}_{t} \mid \boldsymbol{x}_{0} \sim p_{t}(\boldsymbol{x}_{t} \mid \boldsymbol{x}_{0})} \left[ -\left\{ d'\left(s_{q_{sg[\theta], t}}(\boldsymbol{x}_{t}, c) - s_{p_{t}}(\boldsymbol{x}_{t}, c)\right)\right\}^{T} \right]$$

$$\left\{ s_{q_{sg[\theta], t}}(\boldsymbol{x}_{t}, c) - \nabla_{\boldsymbol{x}_{t}} \log p_{t}(\boldsymbol{x}_{t} \mid \boldsymbol{x}_{0}, c) \right\}$$

$$+ d(s_{q_{sg[\theta], t}}(\boldsymbol{x}_{t}, c) - s_{p_{t}}(\boldsymbol{x}_{t}, c))$$

Please refer to supplementary materials for the proof.

According to this theorem, The optimization problem in Eq. 7 and 8 can be formulated as

$$dt \theta^* := \arg \min_{\theta} \mathbb{E} \sum_{\substack{\boldsymbol{x}_0 = g_{\theta}(\boldsymbol{z}, c), \ \boldsymbol{x}_t | \boldsymbol{x}_0 \sim p_t(\boldsymbol{x}_t | \boldsymbol{x}_0)}} [L_{GSIM}(\theta)],$$

$$L_{GSIM} = L_1 + L_2,$$

$$L_1 = -\left\{d'(y_t)\right\}^T \left\{s_{q_{\text{sg}[\theta], t}}(\boldsymbol{x}_t, c) - \nabla_{\boldsymbol{x}_t} \log p_t(\boldsymbol{x}_t | \boldsymbol{x}_0, c)\right\},$$

$$L_2 = d(y_t), \quad y_t = s_{q_{\text{sg}[\theta], t}}(\boldsymbol{x}_t, c) - s_{p_t}(\boldsymbol{x}_t, c),$$
(11)

where  $s_{q_{\mathrm{sg}[ heta],t}}(oldsymbol{x}_t,c)$  can be approximated by the auxiliary network  $\hat{S}_{\phi}(x_t, t, c)$ . Although theory suggests using the

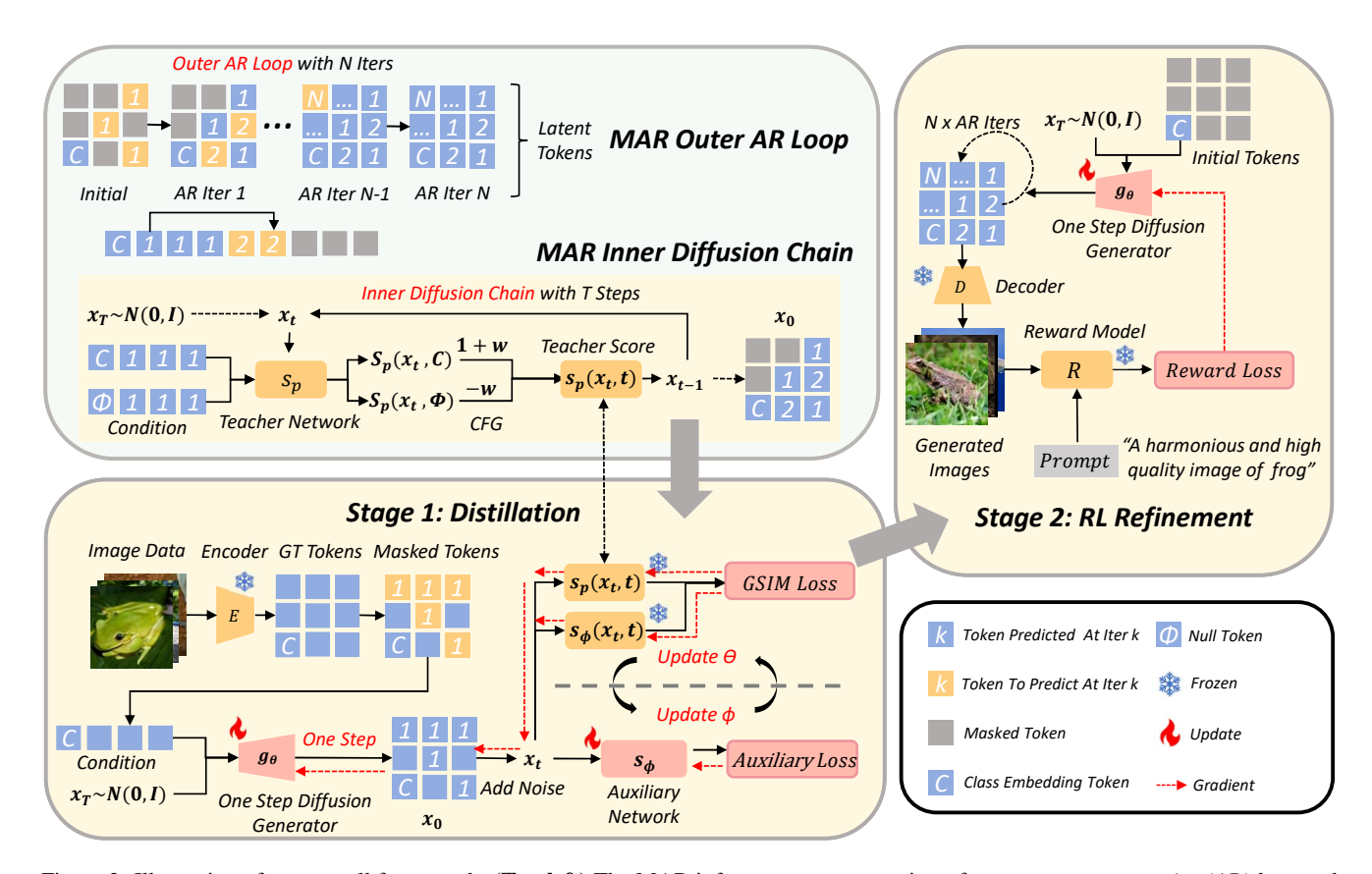


Figure 2. Illustration of our overall framework. (**Top-left**) The MAR inference process consists of an *outer auto-regressive* (AR) loop and an *inner diffusion chain*. Starting from the class embedding token c, MAR performs multiple AR iterations, where each iteration predicts a new subset of latent tokens through a short diffusion process. (**Bottom-left**) The student one-step generator  $g_{\theta}$  and the auxiliary network are optimized alternately. In this stage, a portion of tokens is masked, and  $g_{\theta}$  performs a single AR iteration to predict all masked tokens guided by the teacher MAR model's CFG-based predictions. (**Right**) The RL refinement stage further improves perceptual fidelity. Here, the distilled generator  $g_{\theta}$  generates images through multi-step AR inference, and a reward model evaluates the outputs based on textual prompts. The reward loss then fine-tunes  $g_{\theta}$  to better align with human perceptual preferences.

squared  $\ell_2$  distance  $\|\cdot\|_2^2$  for  $d(\cdot,\cdot)$  in Eq. 8 is necessary to recover the KL objective exactly, in practice this choice can cause training instability. For improved training robustness and faster convergence, we adopt the *Pseudo-Huber distance* as the loss function in our implementation, following [31]. Concretely, in Eq. 11 we set

$$d(y_t) = \sqrt{||y_t||_2^2 + r^2} - r,$$
  

$$d'(y_t) = y_t / \sqrt{||y_t||_2^2 + r^2}$$
(12)

where r is a small constant to avoid division by zero (we use r = 1e - 5).

# 3.2. Reinforcement Learning for Post-Hoc Refinement

Although GSIM efficiently matches the teacher's output distribution, that distribution can still diverge from human perceptual preferences—primarily due to cumulative errors

across the autoregressive loops. To further improve perceptual fidelity, we introduce a reinforcement learning (RL) fine-tuning stage.

However, the RL process cannot be seamlessly integrated with the GSIM distillation phase. The key reason lies in the fundamental difference between MAR's training dynamics and its inference process. During both MAR training and GSIM distillation, the model operates with a fraction of tokens kept unmasked and performs only a **single** auto-regressive (AR) iteration, where the diffusion model predicts all masked tokens conditioned on the visible context *c*. This single-step generation, while sufficient for learning semantic consistency from the teacher, produces low-fidelity images that lack fine perceptual details.

In contrast, MAR inference begins solely from the class embedding  $c_{emb}$  and relies on **multiple** AR iterations to progressively refine image quality. If we were to couple RL with GSIM and directly optimize on single-step samples, the reward model would evaluate these low-quality inter-

mediate outputs rather than the final multi-iteration results. This would lead to misleading gradients and unstable policy optimization, since the reward signal would not correspond to the perceptual quality achieved during inference.

Therefore, RL fine-tuning must be formulated as a separate, post-hoc refinement phase applied to the distilled generator  $g_{\theta}$ . In this stage,  $g_{\theta}$  performs multi-step AR generation consistent with MAR inference, ensuring that the reward feedback reflects the true perceptual quality of the final outputs.

We treat the single-step generator  $g_{\theta}$  as a policy. For a given class  $c_{emb}$ , the policy generates an output with K iterations as illustrated in Eq. 4,  $x_g = G_{\theta}(z, c_{emb}, K)$ , which we consider an "action." We use  $G_{\theta}$  to differ the multi-iteration generation from single-iteration  $g_{\theta}$ . To guide this policy, we employ a pre-trained reward model that provides a scalar score reflecting the alignment between the generated image and the textual context. For specific  $c_{emb}$ , we can get the class name in text, such as 'frog', so we can design the prompt  $prompt_c$  about corresponding class like 'a high-quality and harmonious picture of  $\{class\ name\}$ '. Let this reward function be denoted by  $R(x_g, prompt_c)$ . The RL objective is to maximize the expected reward of the generated outputs, which is achieved by minimizing the following loss function:

$$\mathcal{L}_{RL} = -\mathbb{E}_{c_{emb},z} \left[ R(G_{\theta}(z, c_{emb}, K), prompt_c) \right]$$
 (13)

By back propagating the gradient from this reward signal, we fine-tune  $\theta$  to produce outputs that are not only consistent with the auto-regressive prior but also explicitly optimized for higher quality and better text-image alignment. For our specific implementation, we utilize **PickScore** [23] as the reward model  $R(\cdot)$ , as it is a powerful function known to correlate well with human aesthetic judgments and preferences.

# 4. Experiments

In this section, we evaluate the proposed distillation and reinforcement learning (RL) scheme for our MARVAL (Masked Auto-regressive Variational Acceleration). We conduct three sets of experiments to investigate (1) the influence of classifier-free guidance (CFG) scales on the distilled model, (2) the acceleration achieved over MAR under varying numbers of autoregressive iterations and diffusion steps, (3) the overall effectiveness and significance of RL refinement across models of different scales.

# 4.1. Experimental Setup

**Model Settings** Following MAR [26], our diffusion process adopts a cosine noise schedule with 1000 training steps. The denoising network predicts the noise vector  $\varepsilon$  through a lightweight MLP. We evaluate three model scales

the same as MAR, denoted as **Base**, **Large**, and **Huge**, which differ in the depth and width of the denoising MLP used in the diffusion component. The details of different models are illustrated in **Table 1**. In the distillation stage, we train each model on 8 NVIDIA A800 GPUs for 30 epochs, which takes approximately 3 days to complete. In the RL refinement stage, we further refine the distilled model on the same hardware configuration for 5 epochs, requiring about 2 days of training.

| Model Type | MLP Depth | MLP Width | #Params |
|------------|-----------|-----------|---------|
| Base       | 6         | 1024      | 208M    |
| Large      | 8         | 1280      | 479M    |
| Huge       | 12        | 1536      | 943M    |

Table 1. Different scales of MAR model with diffusion loss. Depth and width refer to the number of residual MLP blocks and hidden channel dimensions respectively.

**Evaluation Metrics.** We evaluate two aspects of performance:

- **Text-image alignment:** measured by **CLIP Score** [14] and **ImageReward Score** [62], using prompts in the form of "a high-quality and harmonious picture of + class name".
- Image quality: measured by Fréchet Inception Distance(FID) [15] and Inception Score (IS) [46].

In order to ensure the robustness and accurate results, all our metrics are tested on 50K generated samples uniformly distributed in 1000 classes corresponding to ImageNet dataset.

#### 4.2. Classifier-Free Guidance Scale in Distillation

According to Eq. 10, we set the Classifier-Free Guidance (CFG) scale w manually during the distillation stage. To study its effect, we vary w for the base MAR model (MAR-B) and evaluate the distilled results using FID and IS.

| Model    | CFG scale (w)   | FID↓  | IS↑   |
|----------|-----------------|-------|-------|
| MARVAL-B | w = 1 (w/o CFG) | 3.75  | 182.1 |
|          | w = 1.2         | 3.06  | 220.2 |
|          | w = 1.5         | 4.24  | 261.7 |
|          | w = 2           | 7.98  | 294.4 |
|          | w = 3           | 11.98 | 317.1 |
|          | w = 4           | 13.84 | 316.8 |
| MAR-B    | w = 2.9         | 2.60  | 222.7 |

Table 2. FID and IS of distilled one-step models under different CFG scales, compared with the optimal setting of MAR-B.

As shown in Table 2, increasing w improves IS, indicating enhanced image fidelity, but overly large w degrades

FID, which suggests sacrificing the diversity and the data alignment for better fidelity. Since ImageNet contains lowquality samples, we aim to balance realism and fidelity rather than minimizing FID alone.

We therefore select w=1.2 as the optimal setting. This choice yields a favorable trade-off between visual sharpness and distribution consistency.

#### 4.3. Effect of Distillation

We further investigate the effect of distillation on the **Base model** by varying the number of auto-regressive iterations  $(N_{\rm AR})$  and diffusion steps  $(N_{\rm diff})$ . As shown in Fig. 3, increasing  $N_{\rm diff}$  gradually improves both FID and IS, while the performance saturates around  $N_{\rm diff}=100$ , consistent with observations in the MAR paper.

After distillation, the one-step model achieves performance comparable to MAR-B under its optimal configuration ( $N_{\rm diff}=100$ ) and even surpasses MAR-B with  $N_{\rm diff}=30$ . This indicates that our distillation effectively preserves the teacher model's generative capability while dramatically simplifying the sampling process.

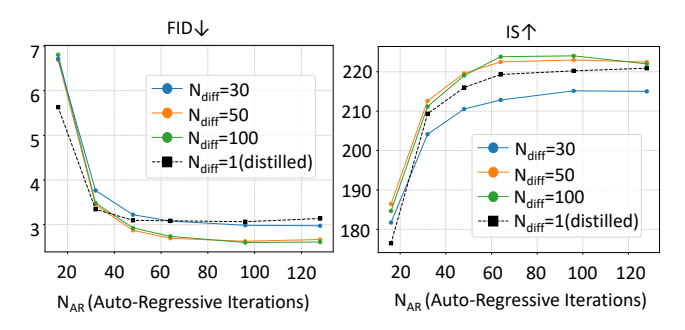


Figure 3. Effect of AR iterations and diffusion steps on FID/IS for the MAR base model compared to MARVAL base model.

We also evaluate the **Large** and **Huge** variants, summarized in Table 3. The MARVAL models maintain better FID than MAR while achieving significantly higher Inception Scores, confirming that distillation improves perceptual quality without compromising data alignment. The FID and IS in Table 3 of MAR and MARVAL are achieved with the optimal settings on NVIDIA A100 GPUs, and the inference time is tested when batch size equals 1 on a single A100 GPU. For the **Base** model, the generation takes only **0.61 seconds** after distillation, compared to **20.10 seconds** of MAR-B. The diffusion sampling process itself is accelerated by nearly **100**×, and considering the auto-regressive component, the overall real time generation speed improves by about **32.95**×. Overall, our MARVAL models perform the best in generation quality and speed.

# 4.4. The Significance of Reinforcement Learning

To assess the impact of reinforcement learning (RL) finetuning, we perform an ablation study comparing models

| Model                    | FID↓ | IS↑   | inference time |
|--------------------------|------|-------|----------------|
| pixel-based              |      |       |                |
| ADM [8]                  | 4.59 | 186.7 | 115.67 s       |
| continuous-valued tokens |      |       |                |
| LDM-4 [44]               | 3.60 | 247.7 | 37.25s         |
| U-ViT-H/2 [1]            | 2.29 | 263.9 | 3.01 s         |
| DiT-XL/2 [38]            | 2.27 | 278.2 | 6.62 s         |
| masked auto-regressive   |      |       |                |
| MAR-B ( $w = 2.9$ )      | 2.60 | 222.7 | 20.10 s        |
| MAR-L ( $w = 3.0$ )      | 2.23 | 240.5 | 24.04 s        |
| MAR-H ( $w = 3.2$ )      | 2.06 | 247.7 | 30.98 s        |
| distilled only           |      |       |                |
| MARVAL-B                 | 3.06 | 220.2 | <b>0.61</b> s  |
| MARVAL-L                 | 2.51 | 247.1 | 0.97 s         |
| MARVAL-H                 | 2.00 | 256.3 | 1.67 s         |

Table 3. System-level comparison on ImageNet 256×256 conditional generation. Our MARVAL model achieves the best performance in FID while requiring the least inference time. All MARVAL models are evaluated with a CFG scale of 1.2, whereas MAR baselines use the CFG settings provided in their official evaluation scripts.

before and after RL optimization. Starting from the distilled model, RL fine-tuning is applied to better align image generation with perceptual and semantic objectives. RL markedly improves visual quality and perceptual realism, as reflected in the significant improvent of reward-based metrics in Table 4.

| Model | Distill w/o RL |        | Distill | w RL   |
|-------|----------------|--------|---------|--------|
|       | CLIP↑          | ImgR↑  | CLIP↑   | ImgR↑  |
| Base  | 29.40          | -0.142 | 29.47   | -0.110 |
| Large | 29.43          | -0.113 | 29.84   | -0.076 |
| Huge  | 29.33          | -0.107 | 29.78   | -0.064 |

Table 4. Reward-based evaluation (CLIP and ImageReward) before and after RL fine-tuning. Higher scores indicate better semantic fidelity and perceptual alignment with human preference.

As illustrated in Fig. 4, RL fine-tuning brings clear improvements across diverse object categories. The MAR-B baseline captures coarse semantics but often produces unrealistic textures and structural distortions—examples such as the *hare* and *diamondback* exhibit oversimplified shapes. Without RL, examples such as the *hare*, *cougar*, and *dowitcher* appear blurry and distorted, while the *diamondback* loses clear boundaries. After RL, main subjects become more salient, contours and textures are better preserved, and the overall composition appears more natural. These results

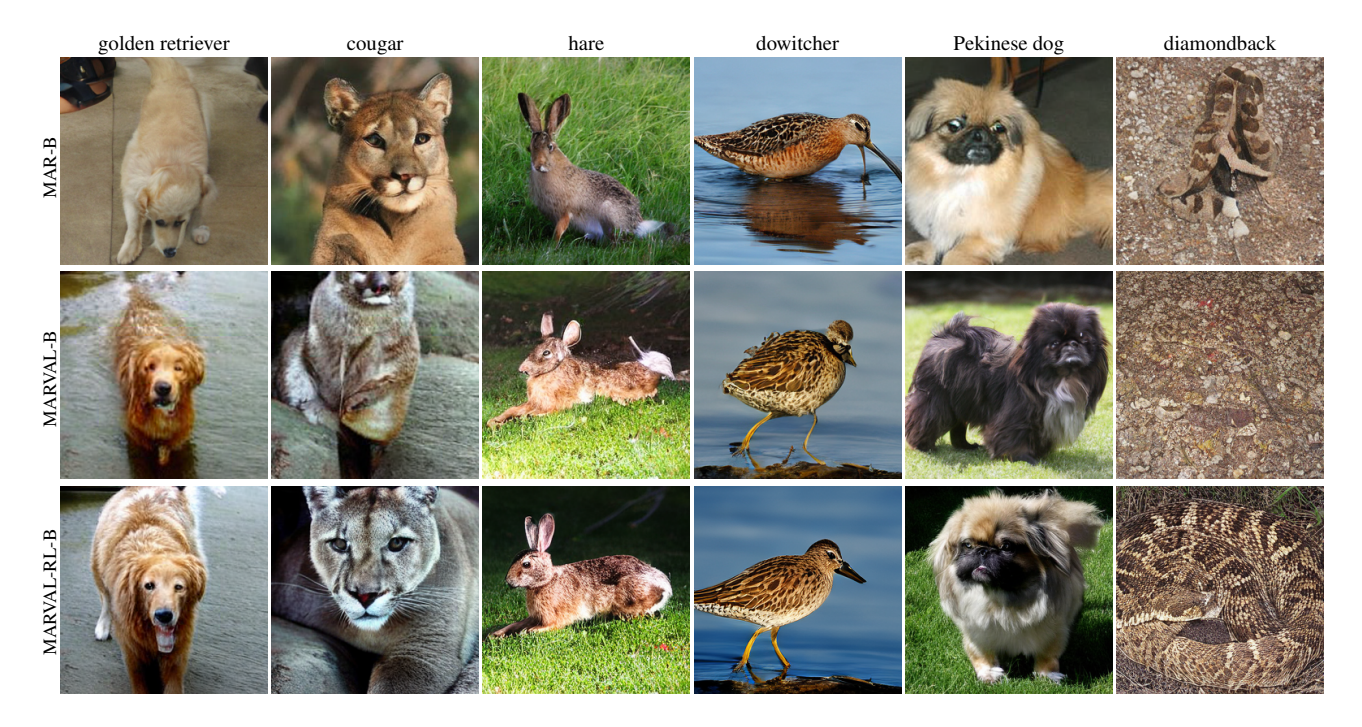


Figure 4. Qualitative comparison among MAR-B, MARVAL-B (without RL), and MARVAL-RL-B. The first row (MAR-B) shows MAR-B generation results, which capture coarse object semantics but often suffer from limited visual realism, noticeable artifacts, and poor texture fidelity. The second row (MARVAL-B) shows that images generated by the distilled one-step model tend to be smoother and less detailed—animal faces appear blurred or distorted, and fine-grained textures or contextual cues are frequently lost. The third row (MARVAL-RL-B) demonstrates the effect of reinforcement learning refinement: details such as fur texture, feather edges, and body contours become significantly sharper and more coherent. The enhanced structure and perceptual realism highlight RL as an essential stage for aligning the model's outputs with human visual preferences.

confirm that RL guides the model toward sharper, semantically faithful, and perceptually coherent outputs, successfully enhancing the distilled model despite minor metric degradations. Overall, these results confirm that RL finetuning effectively enhances image fidelity and perceptual quality, demonstrating the success of our approach.

#### 5. Conclusion

In this work, we addressed the fundamental limitations of Masked Auto-Regressive (MAR) models—slow inference and the infeasibility of fine-tuning with reinforcement learning—by proposing a unified variational acceleration framework, GSIM. Built upon the novel score-based variational principle, our method distills the costly diffusion denoising chains in MAR into a single-step generator, dramatically improving inference efficiency while preserving the auto-regressive ordering.

This acceleration not only alleviates the computational bottleneck of MAR models but also enables effective post-training with reinforcement learning, which was previously impractical due to excessive computational costs. Leveraging human preference rewards, our MARVAL-RL model achieves both over 30× acceleration and better alignment

with perceptual quality and semantic fidelity compared to conventional MAR diffusion decoding.

Limitations and Future Directions Our work enables efficient generation and practical RL post-training for MAR models, but its RL stage still requires multi-step AR iterations together with a large reward model. This overhead imposes substantial memory demands, which consequently restricts the feasible batch size in the RL stage. This effect becomes increasingly pronounced as the model scales up, leading to less efficient RL refinement. A practical mitigation is to shrink the active training graph, such as using lighter reward models or reducing AR iterations appropriately to relieve memory pressure and improve efficiency.

A natural extension of our distillation + RL framework is applying it to other AR + diffusion architectures beyond the class-conditional image generation of MAR. In particular, the same principles could benefit large text-to-image systems and multi-modal AR models, enabling faster sampling and more efficient preference optimization. Exploring these directions may provide a broader validation of the generality and cross-modal applicability of our approach.

#### References

- [1] Fan Bao, Chongxuan Li, Yue Cao, and Jun Zhu. All are worth words: a vit backbone for score-based diffusion models. In NeurIPS 2022 Workshop on Score-Based Methods, 2022. 7
- [2] David Berthelot, Arnaud Autef, Jierui Lin, Dian Ang Yap, Shuangfei Zhai, Siyuan Hu, Daniel Zheng, Walter Talbott, and Eric Gu. Tract: Denoising diffusion models with transitive closure time-distillation. arXiv preprint arXiv:2303.04248, 2023. 3
- [3] Kevin Black, Michael Janner, Yilun Du, Ilya Kostrikov, and Sergey Levine. Training diffusion models with reinforcement learning. arXiv preprint arXiv:2305.13301, 2023. 3
- [4] Paul F Christiano, Jan Leike, Tom Brown, Miljan Martic, Shane Legg, and Dario Amodei. Deep reinforcement learning from human preferences. *Advances in neural information processing systems*, 30, 2017. 1
- [5] Kevin Clark, Paul Vicol, Kevin Swersky, and David J Fleet. Directly fine-tuning diffusion models on differentiable rewards. *arXiv preprint arXiv:2309.17400*, 2023. 3
- [6] Xiaoliang Dai, Ji Hou, Chih-Yao Ma, Sam Tsai, Jialiang Wang, Rui Wang, Peizhao Zhang, Simon Vandenhende, Xiaofang Wang, Abhimanyu Dubey, et al. Emu: Enhancing image generation models using photogenic needles in a haystack. arXiv preprint arXiv:2309.15807, 2023. 3
- [7] Jia Deng, Wei Dong, Richard Socher, Li-Jia Li, Kai Li, and Li Fei-Fei. Imagenet: A large-scale hierarchical image database. In 2009 IEEE conference on computer vision and pattern recognition, pages 248–255. Ieee, 2009. 1
- [8] Prafulla Dhariwal and Alexander Nichol. Diffusion models beat gans on image synthesis. *Advances in neural information processing systems*, 34:8780–8794, 2021. 1, 7
- [9] Patrick Esser, Robin Rombach, and Bjorn Ommer. Taming transformers for high-resolution image synthesis. In *Proceedings of the IEEE/CVF conference on computer vision and pattern recognition*, pages 12873–12883, 2021.
- [10] Ying Fan, Olivia Watkins, Yuqing Du, Hao Liu, Moonkyung Ryu, Craig Boutilier, Pieter Abbeel, Mohammad Ghavamzadeh, Kangwook Lee, and Kimin Lee. Reinforcement learning for fine-tuning text-to-image diffusion models. Advances in Neural Information Processing Systems, 36, 2024. 3
- [11] Zhengyang Geng, Ashwini Pokle, William Luo, Justin Lin, and J Zico Kolter. Consistency models made easy. arXiv preprint arXiv:2406.14548, 2024. 3
- [12] Shuyang Gu, Dong Chen, Jianmin Bao, Fang Wen, Bo Zhang, Dongdong Chen, Lu Yuan, and Baining Guo. Vector quantized diffusion model for text-to-image synthesis. In *Proceedings of the IEEE/CVF conference on computer vision and pattern recognition*, pages 10696–10706, 2022. 1
- [13] Jonathan Heek, Emiel Hoogeboom, and Tim Salimans. Multistep consistency models. arXiv preprint arXiv:2403.06807, 2024. 3
- [14] Jack Hessel, Ari Holtzman, Maxwell Forbes, Ronan Le Bras, and Yejin Choi. Clipscore: A reference-free evaluation metric for image captioning. arXiv preprint arXiv:2104.08718, 2021. 6

- [15] Martin Heusel, Hubert Ramsauer, Thomas Unterthiner, Bernhard Nessler, and Sepp Hochreiter. Gans trained by a two time-scale update rule converge to a local nash equilibrium. Advances in neural information processing systems, 30, 2017. 6
- [16] Jonathan Ho and Tim Salimans. Classifier-free diffusion guidance. arXiv preprint arXiv:2207.12598, 2022. 4
- [17] Jonathan Ho, Ajay Jain, and Pieter Abbeel. Denoising diffusion probabilistic models. *Advances in neural information processing systems*, 33:6840–6851, 2020. 1, 2
- [18] Jiwoo Hong, Sayak Paul, Noah Lee, Kashif Rasul, James Thorne, and Jongheon Jeong. Margin-aware preference optimization for aligning diffusion models without reference. In First Workshop on Scalable Optimization for Efficient and Adaptive Foundation Models, 2024. 3
- [19] Emiel Hoogeboom, Alexey A Gritsenko, Jasmijn Bastings, Ben Poole, Rianne van den Berg, and Tim Salimans. Autoregressive diffusion models. arXiv preprint arXiv:2110.02037, 2021. 1
- [20] Tero Karras, Miika Aittala, Timo Aila, and Samuli Laine. Elucidating the design space of diffusion-based generative models. Advances in neural information processing systems, 35:26565–26577, 2022. 3
- [21] Dongjun Kim, Chieh-Hsin Lai, Wei-Hsiang Liao, Naoki Murata, Yuhta Takida, Toshimitsu Uesaka, Yutong He, Yuki Mitsufuji, and Stefano Ermon. Consistency trajectory models: Learning probability flow ode trajectory of diffusion. arXiv preprint arXiv:2310.02279, 2023. 3
- [22] Diederik P Kingma and Max Welling. Auto-encoding variational bayes. *arXiv preprint arXiv:1312.6114*, 2013. 3
- [23] Yuval Kirstain, Adam Polyak, Uriel Singer, Shahbuland Matiana, Joe Penna, and Omer Levy. Pick-a-pic: An open dataset of user preferences for text-to-image generation. Advances in neural information processing systems, 36:36652–36663, 2023. 6, 2
- [24] Kimin Lee, Hao Liu, Moonkyung Ryu, Olivia Watkins, Yuqing Du, Craig Boutilier, Pieter Abbeel, Mohammad Ghavamzadeh, and Shixiang Shane Gu. Aligning textto-image models using human feedback. arXiv preprint arXiv:2302.12192, 2023. 3
- [25] Jiachen Li, Weixi Feng, Wenhu Chen, and William Yang Wang. Reward guided latent consistency distillation. *arXiv* preprint arXiv:2403.11027, 2024. 3
- [26] Tianhong Li, Yonglong Tian, He Li, Mingyang Deng, and Kaiming He. Autoregressive image generation without vector quantization. *Advances in Neural Information Processing Systems*, 37:56424–56445, 2024. 1, 3, 6
- [27] Cheng Lu, Yuhao Zhou, Fan Bao, Jianfei Chen, Chongxuan Li, and Jun Zhu. Dpm-solver: A fast ode solver for diffusion probabilistic model sampling in around 10 steps. *arXiv* preprint arXiv:2206.00927, 2022. 3
- [28] Weijian Luo. A comprehensive survey on knowledge distillation of diffusion models. arXiv preprint arXiv:2304.04262, 2023. 3
- [29] Weijian Luo. Diff-instruct++: Training one-step text-to-image generator model to align with human preferences. arXiv preprint arXiv:2410.18881, 2024. 3

- [30] Weijian Luo, Tianyang Hu, Shifeng Zhang, Jiacheng Sun, Zhenguo Li, and Zhihua Zhang. Diff-instruct: A universal approach for transferring knowledge from pre-trained diffusion models. Advances in Neural Information Processing Systems, 36, 2024. 3
- [31] Weijian Luo, Zemin Huang, Zhengyang Geng, J Zico Kolter, and Guo-jun Qi. One-step diffusion distillation through score implicit matching. Advances in Neural Information Processing Systems, 37:115377–115408, 2024. 3, 5
- [32] Weijian Luo, Colin Zhang, Debing Zhang, and Zhengyang Geng. David and goliath: Small one-step model beats large diffusion with score post-training. *arXiv preprint arXiv:2410.20898*, 2024. 3
- [33] Weijian Luo, Colin Zhang, Debing Zhang, and Zhengyang Geng. Diff-instruct\*: Towards human-preferred one-step text-to-image generative models. *arXiv e-prints*, pages arXiv–2410, 2024.
- [34] Yihong Luo, Tianyang Hu, Weijian Luo, Kenji Kawaguchi, and Jing Tang. Reward-instruct: A reward-centric approach to fast photo-realistic image generation. *arXiv preprint arXiv:2503.13070*, 2025. 3
- [35] Minh-Thang Luong, Hieu Pham, and Christopher D Manning. Effective approaches to attention-based neural machine translation. *arXiv* preprint arXiv:1508.04025, 2015. 1
- [36] Chenlin Meng, Ruiqi Gao, Diederik P Kingma, Stefano Ermon, Jonathan Ho, and Tim Salimans. On distillation of guided diffusion models. arXiv preprint arXiv:2210.03142, 2022. 3
- [37] Long Ouyang, Jeffrey Wu, Xu Jiang, Diogo Almeida, Carroll Wainwright, Pamela Mishkin, Chong Zhang, Sandhini Agarwal, Katarina Slama, Alex Ray, et al. Training language models to follow instructions with human feedback. Advances in neural information processing systems, 35:27730–27744, 2022. 1
- [38] William Peebles and Saining Xie. Scalable diffusion models with transformers. In Proceedings of the IEEE/CVF international conference on computer vision, pages 4195–4205, 2023. 7
- [39] Dustin Podell, Zion English, Kyle Lacey, Andreas Blattmann, Tim Dockhorn, Jonas Müller, Joe Penna, and Robin Rombach. Sdxl: Improving latent diffusion models for high-resolution image synthesis. *arXiv preprint arXiv:2307.01952*, 2023. 3
- [40] Mihir Prabhudesai, Anirudh Goyal, Deepak Pathak, and Katerina Fragkiadaki. Aligning text-to-image diffusion models with reward backpropagation. arXiv preprint arXiv:2310.03739, 2023. 3
- [41] Aditya Ramesh, Mikhail Pavlov, Gabriel Goh, Scott Gray, Chelsea Voss, Alec Radford, Mark Chen, and Ilya Sutskever. Zero-shot text-to-image generation. In *International conference on machine learning*, pages 8821–8831. Pmlr, 2021. 1
- [42] Scott Reed, Yutian Chen, Thomas Paine, Aäron van den Oord, SM Eslami, Danilo Rezende, Oriol Vinyals, and Nando de Freitas. Few-shot autoregressive density estimation: Towards learning to learn distributions. *arXiv preprint arXiv:1710.10304*, 2017. 1
- [43] Scott Reed, Aäron Oord, Nal Kalchbrenner, Sergio Gómez Colmenarejo, Ziyu Wang, Yutian Chen, Dan Belov, and

- Nando Freitas. Parallel multiscale autoregressive density estimation. In *International conference on machine learning*, pages 2912–2921. PMLR, 2017. 1
- [44] Robin Rombach, Andreas Blattmann, Dominik Lorenz, Patrick Esser, and Björn Ommer. High-resolution image synthesis with latent diffusion models. In *Proceedings of* the IEEE/CVF conference on computer vision and pattern recognition, pages 10684–10695, 2022. 7
- [45] Tim Salimans and Jonathan Ho. Progressive distillation for fast sampling of diffusion models. arXiv preprint arXiv:2202.00512, 2022. 3
- [46] Tim Salimans, Ian Goodfellow, Wojciech Zaremba, Vicki Cheung, Alec Radford, and Xi Chen. Improved techniques for training gans. Advances in neural information processing systems, 29, 2016. 1, 6
- [47] Tim Salimans, Thomas Mensink, Jonathan Heek, and Emiel Hoogeboom. Multistep distillation of diffusion models via moment matching. arXiv preprint arXiv:2406.04103, 2024.
- [48] Axel Sauer, Dominik Lorenz, Andreas Blattmann, and Robin Rombach. Adversarial diffusion distillation. arXiv preprint arXiv:2311.17042, 2023. 3
- [49] Jiaming Song, Chenlin Meng, and Stefano Ermon. Denoising diffusion implicit models. arXiv preprint arXiv:2010.02502, 2020. 1, 2, 3
- [50] Yang Song and Prafulla Dhariwal. Improved techniques for training consistency models. In *The Twelfth International Conference on Learning Representations*, 2024. 3
- [51] Yang Song and Stefano Ermon. Generative modeling by estimating gradients of the data distribution. *Advances in neural information processing systems*, 32, 2019. 2
- [52] Yang Song, Jascha Sohl-Dickstein, Diederik P Kingma, Abhishek Kumar, Stefano Ermon, and Ben Poole. Score-based generative modeling through stochastic differential equations. *arXiv preprint arXiv:2011.13456*, 2020. 1, 2, 3
- [53] Yang Song, Prafulla Dhariwal, Mark Chen, and Ilya Sutskever. Consistency models. 2023. 3
- [54] Nisan Stiennon, Long Ouyang, Jeffrey Wu, Daniel Ziegler, Ryan Lowe, Chelsea Voss, Alec Radford, Dario Amodei, and Paul F Christiano. Learning to summarize with human feedback. Advances in neural information processing systems, 33:3008–3021, 2020. 1
- [55] Keyu Tian, Yi Jiang, Zehuan Yuan, Bingyue Peng, and Liwei Wang. Visual autoregressive modeling: Scalable image generation via next-scale prediction. Advances in neural information processing systems, 37:84839–84865, 2024.
- [56] Aaron Van den Oord, Nal Kalchbrenner, Lasse Espeholt, Oriol Vinyals, Alex Graves, et al. Conditional image generation with pixelcnn decoders. Advances in neural information processing systems, 29, 2016.
- [57] Aäron Van Den Oord, Nal Kalchbrenner, and Koray Kavukcuoglu. Pixel recurrent neural networks. In *International conference on machine learning*, pages 1747–1756. PMLR, 2016. 1
- [58] Pascal Vincent. A connection between score matching and denoising autoencoders. *Neural computation*, 23(7):1661– 1674, 2011. 1

- [59] Bram Wallace, Meihua Dang, Rafael Rafailov, Linqi Zhou, Aaron Lou, Senthil Purushwalkam, Stefano Ermon, Caiming Xiong, Shafiq Joty, and Nikhil Naik. Diffusion model alignment using direct preference optimization. In *Proceedings of* the IEEE/CVF Conference on Computer Vision and Pattern Recognition, pages 8228–8238, 2024. 3
- [60] Yifei Wang, Weimin Bai, Colin Zhang, Debing Zhang, Weijian Luo, and He Sun. Uni-instruct: One-step diffusion model through unified diffusion divergence instruction. arXiv preprint arXiv:2505.20755, 2025. 3, 4
- [61] Sirui Xie, Zhisheng Xiao, Diederik P Kingma, Tingbo Hou, Ying Nian Wu, Kevin Patrick Murphy, Tim Salimans, Ben Poole, and Ruiqi Gao. Em distillation for one-step diffusion models. arXiv preprint arXiv:2405.16852, 2024. 3
- [62] Jiazheng Xu, Xiao Liu, Yuchen Wu, Yuxuan Tong, Qinkai Li, Ming Ding, Jie Tang, and Yuxiao Dong. Imagereward: Learning and evaluating human preferences for texto-image generation. Advances in Neural Information Processing Systems, 36:15903–15935, 2023. 6
- [63] Yanwu Xu, Yang Zhao, Zhisheng Xiao, and Tingbo Hou. Ufogen: You forward once large scale text-to-image generation via diffusion gans. In *Proceedings of the IEEE/CVF Conference on Computer Vision and Pattern Recognition*, pages 8196–8206, 2024. 3
- [64] Shuchen Xue, Mingyang Yi, Weijian Luo, Shifeng Zhang, Jiacheng Sun, Zhenguo Li, and Zhi-Ming Ma. Sa-solver: Stochastic adams solver for fast sampling of diffusion models. Advances in Neural Information Processing Systems, 36: 77632–77674, 2023. 3
- [65] Kai Yang, Jian Tao, Jiafei Lyu, Chunjiang Ge, Jiaxin Chen, Weihan Shen, Xiaolong Zhu, and Xiu Li. Using human feedback to fine-tune diffusion models without any reward model. In Proceedings of the IEEE/CVF Conference on Computer Vision and Pattern Recognition, pages 8941– 8951, 2024. 3
- [66] Tianwei Yin, Michaël Gharbi, Richard Zhang, Eli Shechtman, Fredo Durand, William T Freeman, and Taesung Park. One-step diffusion with distribution matching distillation. arXiv preprint arXiv:2311.18828, 2023. 3
- [67] Jianbin Zheng, Minghui Hu, Zhongyi Fan, Chaoyue Wang, Changxing Ding, Dacheng Tao, and Tat-Jen Cham. Trajectory consistency distillation. arXiv preprint arXiv:2402.19159, 2024.
- [68] Mingyuan Zhou, Zhendong Wang, Huangjie Zheng, and Hai Huang. Long and short guidance in score identity distillation for one-step text-to-image generation. arXiv preprint arXiv:2406.01561, 2024.
- [69] Mingyuan Zhou, Huangjie Zheng, Zhendong Wang, Mingzhang Yin, and Hai Huang. Score identity distillation: Exponentially fast distillation of pretrained diffusion models for one-step generation. In Forty-first International Conference on Machine Learning, 2024. 3, 1, 2

# Masked Auto-Regressive Variational Acceleration: Fast Inference Makes Practical Reinforcement Learning

# Supplementary Material

# 1. Theory Part

In this section we present a detailed proof of the Gradient Equivalent Theorem. The proof of the Gradient Equivalent Theorem is based on the so-called **Score-projection identity** which was first found in [58] to bridge denoising score matching and denoising auto-encoders. Later the identity is applied for deriving distillation methods based on Fisher divergences [69]. We appreciate the efforts of Zhou et al. [69] and re-write the score-projection identity here without proof. Readers can check Zhou et al. [69] for a complete proof of score-projection identity.

**Score-projection identity.** Let  $u(\cdot, \theta)$  be a vector-valued function, using the notations of the Gradient Equivalent Theorem, under mild conditions, the identity holds:

$$\mathbb{E}_{\boldsymbol{x}_{t}|\boldsymbol{x}_{0} \sim p_{t}(\boldsymbol{x}_{t}|\boldsymbol{x}_{0})}^{\boldsymbol{x}_{0} \sim q_{\theta,0}} \left[ f(\boldsymbol{x}_{t}, \boldsymbol{x}_{0}, \theta) \right] = 0, \quad \forall \theta$$

$$f(\boldsymbol{x}_{t}, \boldsymbol{x}_{0}, \theta) = u(\boldsymbol{x}_{t}, \theta)^{T} \left\{ s_{q_{\theta,t}}(\boldsymbol{x}_{t}, c) - \nabla_{\boldsymbol{x}_{t}} \log p_{t}(\boldsymbol{x}_{t}|\boldsymbol{x}_{0}, c) \right\}.$$

Next, we turn to prove the Gradient Equivalent Theorem.

**Proof of Gradient Equivalent Theorem.** We start by applying the chain rule for the total derivative with respect to  $\theta$ . The function  $d(\cdot)$  depends on  $\theta$  both directly through the score function  $s_{q_{\theta,t}}$  and indirectly through the distribution  $x_t \sim q_{\theta,t}$  (as  $x_t$  depends on  $x_0 \sim q_{\theta,0}$ ). This gives two terms:

$$\mathbb{E}_{\boldsymbol{x}_{t} \sim q_{\theta, t}} \frac{\partial}{\partial \theta} d\left(s_{q_{\theta, t}}(\boldsymbol{x}_{t}, c) - s_{p_{t}}(\boldsymbol{x}_{t}, c)\right)$$

$$= \mathbb{E}_{\boldsymbol{x}_{t} \sim q_{\theta, t}} \left[ d'\left(s_{q_{\theta, t}}(\boldsymbol{x}_{t}, c) - s_{p_{t}}(\boldsymbol{x}_{t}, c)\right)^{T} \frac{\partial}{\partial \theta} s_{q_{\theta, t}}(\boldsymbol{x}_{t}, c) + \frac{\partial}{\partial \boldsymbol{x}_{t}} d(s_{q_{\theta, t}}(\boldsymbol{x}_{t}, c) - s_{p_{t}}(\boldsymbol{x}_{t}, c)) \frac{\partial \boldsymbol{x}_{t}}{\partial \theta} \right]$$
(A.2)

We differentiate (A.1) on both sides w.r.t  $\theta$  to achieve the equivalent of the first term in (A.2). Since the expectation is zero for all  $\theta$ , its derivative is also zero. We apply the total derivative (multivariate chain rule), noting that f depends on  $\theta$  directly, as well as indirectly through  $x_0$  and  $x_t$  (both

depend on  $\theta$ ):

$$0 = \frac{\partial}{\partial \theta} \mathbb{E}_{\boldsymbol{x}_{t} | \boldsymbol{x}_{0} \sim q_{\theta,0}} \left[ f(\boldsymbol{x}_{t}, \boldsymbol{x}_{0}, \theta) \right]$$
(A.3)  

$$= \mathbb{E} \left[ \frac{\partial f}{\partial \boldsymbol{x}_{0}} \frac{\partial \boldsymbol{x}_{0}}{\partial \theta} + \frac{\partial f}{\partial \boldsymbol{x}_{t}} \frac{\partial \boldsymbol{x}_{t}}{\partial \theta} + \frac{\partial f}{\partial \theta} \right]$$
(A.4)  

$$= \mathbb{E} \left[ \frac{\partial}{\partial \boldsymbol{x}_{0}} \left\{ u(\boldsymbol{x}_{t}, \theta)^{T} \left\{ -\nabla_{\boldsymbol{x}_{t}} \log p_{t}(\boldsymbol{x}_{t} | \boldsymbol{x}_{0}, c) \right\} \right\} \frac{\partial \boldsymbol{x}_{0}}{\partial \theta}$$
(A.5)  

$$+ \frac{\partial}{\partial \boldsymbol{x}_{t}} \left\{ u(\boldsymbol{x}_{t}, \theta)^{T} \left\{ s_{q_{\theta, t}}(\boldsymbol{x}_{t}, c) - \nabla_{\boldsymbol{x}_{t}} \log p_{t}(\boldsymbol{x}_{t} | \boldsymbol{x}_{0}, c) \right\} \right\} \frac{\partial \boldsymbol{x}_{t}}{\partial \theta}$$
(A.5)  

$$+ \frac{\partial}{\partial \theta} u(\boldsymbol{x}_{t}, \theta)^{T} \left\{ s_{q_{\theta, t}}(\boldsymbol{x}_{t}, c) + u(\boldsymbol{x}_{t}, \theta)^{T} \frac{\partial}{\partial \theta} \left\{ s_{q_{\theta, t}}(\boldsymbol{x}_{t}, c) \right\} \right]$$
  

$$= \mathbb{E} \left[ \frac{\partial}{\partial \theta} \left\{ u(\boldsymbol{x}_{t}, \theta)^{T} \left\{ s_{q_{\text{sg}[\theta], t}}(\boldsymbol{x}_{t}, c) - \nabla_{\boldsymbol{x}_{t}} \log p_{t}(\boldsymbol{x}_{t} | \boldsymbol{x}_{0}, c) \right\} \right\} \right\}$$
  

$$+ u(\boldsymbol{x}_{t}, \theta)^{T} \frac{\partial}{\partial \theta} \left\{ s_{q_{\theta, t}}(\boldsymbol{x}_{t}, c) \right\}.$$
(A.6)

By rearranging the terms in (A.4) and (A.5), and by applying the stop-gradient operator sg to  $s_{q_{\theta,t}}$  within the derivative terms, the expression can be consolidated into (A.6). We then rewrite (A.6) as follows:

$$\mathbb{E}_{x_t \sim q_{\theta,t}} u(\boldsymbol{x}_t, \theta)^T \frac{\partial}{\partial \theta} \{ s_{q_{\theta,t}}(\boldsymbol{x}_t, c) \}$$

$$= -\frac{\partial}{\partial \theta} \mathbb{E}_{\boldsymbol{x}_t | \boldsymbol{x}_0 \sim p_t(\boldsymbol{x}_t | \boldsymbol{x}_0)} \{ u(x_t, \theta)^T \}$$

$$\{ s_{q_{\text{sg}[\theta],t}}(x_t, c) - \nabla_{x_t} \log p_t(x_t | x_0, c) \}$$
(A.7)

Let  $u(\boldsymbol{x}_t, \theta) = d' \left( s_{q_{\text{sg}[\theta],t}}(\boldsymbol{x}_t, c) - s_{p_t}(\boldsymbol{x}_t, c) \right)$  and substitute this specific function u into the identity (A.7):

$$\mathbb{E}_{x_{t} \sim q_{\theta, t}} \left[ d' \left( s_{q_{\text{sg}[\theta], t}}(\boldsymbol{x}_{t}, c) - s_{p_{t}}(\boldsymbol{x}_{t}, c) \right)^{T} \frac{\partial}{\partial \theta} \left\{ s_{q_{\theta, t}}(\boldsymbol{x}_{t}, c) \right\} \right]$$

$$(A.8)$$

$$= \mathbb{E}_{x_{t} \sim q_{\theta, t}} \left[ d' \left( s_{q_{\theta, t}}(\boldsymbol{x}_{t}, c) - s_{p_{t}}(\boldsymbol{x}_{t}, c) \right)^{T} \frac{\partial}{\partial \theta} \left\{ s_{q_{\theta, t}}(\boldsymbol{x}_{t}, c) \right\} \right]$$

$$(A.9)$$

$$= -\frac{\partial}{\partial \theta} \mathbb{E}_{\boldsymbol{x}_{t} \mid \boldsymbol{x}_{0} \sim q_{\theta, 0}} \left\{ d' \left( s_{q_{\text{sg}[\theta], t}}(\boldsymbol{x}_{t}, c) - s_{p_{t}}(\boldsymbol{x}_{t}, c) \right)^{T} \right.$$

$$\left\{ s_{q_{\text{sg}[\theta], t}}(\boldsymbol{x}_{t}, c) - \nabla_{\boldsymbol{x}_{t}} \log p_{t}(\boldsymbol{x}_{t} \mid \boldsymbol{x}_{0}, c) \right\} \right\}$$

$$(A.10)$$

Since  $\theta$  does not participate in the derivative of  $d(\cdot)$ , equation (A.8) is equivalent to (A.9). Moreover,  $\theta$  does not

appear in the differentiation with respect to  $x_t$ :

$$\mathbb{E}_{x_{t} \sim q_{\theta, t}} \left[ \frac{\partial}{\partial \boldsymbol{x}_{t}} d(s_{q_{\theta, t}}(\boldsymbol{x}_{t}, c) - s_{p_{t}}(\boldsymbol{x}_{t}, c)) \frac{\partial \boldsymbol{x}_{t}}{\partial \theta} \right] =$$

$$- \frac{\partial}{\partial \theta} \mathbb{E}_{\boldsymbol{x}_{t} | \boldsymbol{x}_{0} \sim p_{t}(\boldsymbol{x}_{t} | \boldsymbol{x}_{0})} \left[ d\left(s_{q_{\text{sg}[\theta], t}}(\boldsymbol{x}_{t}, c) - s_{p_{t}}(\boldsymbol{x}_{t}, c)\right) \right]$$
(A.11)

By combining (A.10) and (A.11) into (A.2), we get exactly the **Gradient Equivalent Theorem** stated in the text. This completes the proof.

# 2. Implementation Details

In this section, we provide detailed hyperparameter settings and the algorithmic procedure for MARVAL. Our framework consists of two distinct stages: the Guided Score Implicit Matching (GSIM) distillation stage and the Reinforcement Learning (RL) refinement stage.

# 2.1. Hyperparameter Settings

**Model Architectures.** The architecture of our one-step generator follows the same configuration of the original MAR models [69]. The detailed specifications for the Denoising MLP used in the diffusion component are listed in Table 1.

| Hyperparameter             | Stage 1: GSIM Distillation     |
|----------------------------|--------------------------------|
| GPUs                       | $8 \times NVIDIA A100$         |
| Training Epochs            | 30                             |
| Approx. Training Time      | $\sim$ 3 days                  |
| Teacher Steps $(N_{diff})$ | 1000                           |
| Student Steps $(N_{diff})$ | 1                              |
| CFG Scale (w)              | 1.2                            |
| Loss Function              | Pseudo-Huber ( $r = 10^{-5}$ ) |
| Student model Lr           | 5e-6                           |
| Auxiliary model Lr         | 5e-6                           |
| EMA momentum               | 0.9999                         |
| batch size per GPU         | 64                             |

Table 1. Training Settings for MARVAL Distillation stage.

**Training Configurations.** The training is conducted on NVIDIA A100 GPUs. We utilize the AdamW optimizer for both stages. The specific hyperparameters for the Distillation and RL stages are provided in Table 1 and Table 2.

During the distillation stage, we set the teacher's full diffusion steps to  $N_{diff}=1000$  and the one-step generator predicts the noise from the fix step 400. Based on our ablation study, we set the Classifier-Free Guidance (CFG) scale w=1.2 for the teacher score, which provides the optimal trade-off between fidelity (FID) and fidelity. For the loss

| Hyperparameter             | Stage 2: RL Refinement |
|----------------------------|------------------------|
| GPUs                       | 8 × NVIDIA A100        |
| Training Epochs            | 5                      |
| Approx. Training Time      | $\sim$ 2 days          |
| AR Loops $(N_{AR})$        | 64                     |
| Student Steps $(N_{diff})$ | 1                      |
| Reward Model               | Pickscore              |
| Student model Lr           | 5e-6                   |
| EMA momentum               | 0.9999                 |
| batch size per GPU         | 2                      |

Table 2. Training Settings for RL Refinement stage.

function, we use the Pseudo-Huber distance with r = 1e-5 to ensure numerical stability.

During the RL refinement stage, we use PickScore [23] as the reward model. We generate samples with AR loops( $N_{AR}$ )=64 to calculate rewards, ensuring the optimization aligns with the final inference quality and requires less memory costs. Our best results in FID and IS are tested when inferring with  $N_{AR}=128$ .

## 3. Additional Results

This section provides additional qualitative results for the MARVAL-RL-L and MARVAL-RL-H models. These results were not included in the main paper for the following reasons:

- First, due to space limitations, we primarily presented results using the MARVAL-RL-B model.
- Second, the qualitative visualizations in the main experiments adopt MARVAL-RL-B because it already delivers strong visual quality while maintaining the fastest inference speed among all model sizes.
- Third, the MARVAL-L and MARVAL-H models achieve relatively strong performance even before RL fine-tuning, making the improvements brought by RL most pronounced and interpretable on MARVAL-B.

For completeness, we include the MARVAL-RL-L and MARVAL-RL-H visualizations in Fig. 1 and Fig. 2, respectively. Compared with MARVAL-RL-B and MARVAL-RL-L, the MARVAL-RL-H samples exhibit significantly richer fine-grained textures, particularly on man-made objects such as buildings, tools, and clothes. This trend provides additional evidence that our method scales effectively: as model capacity increases, the RL fine-tuning yields increasingly detailed and visually faithful results.



Figure 1. Qualitative results of MARVAL-RL-L.

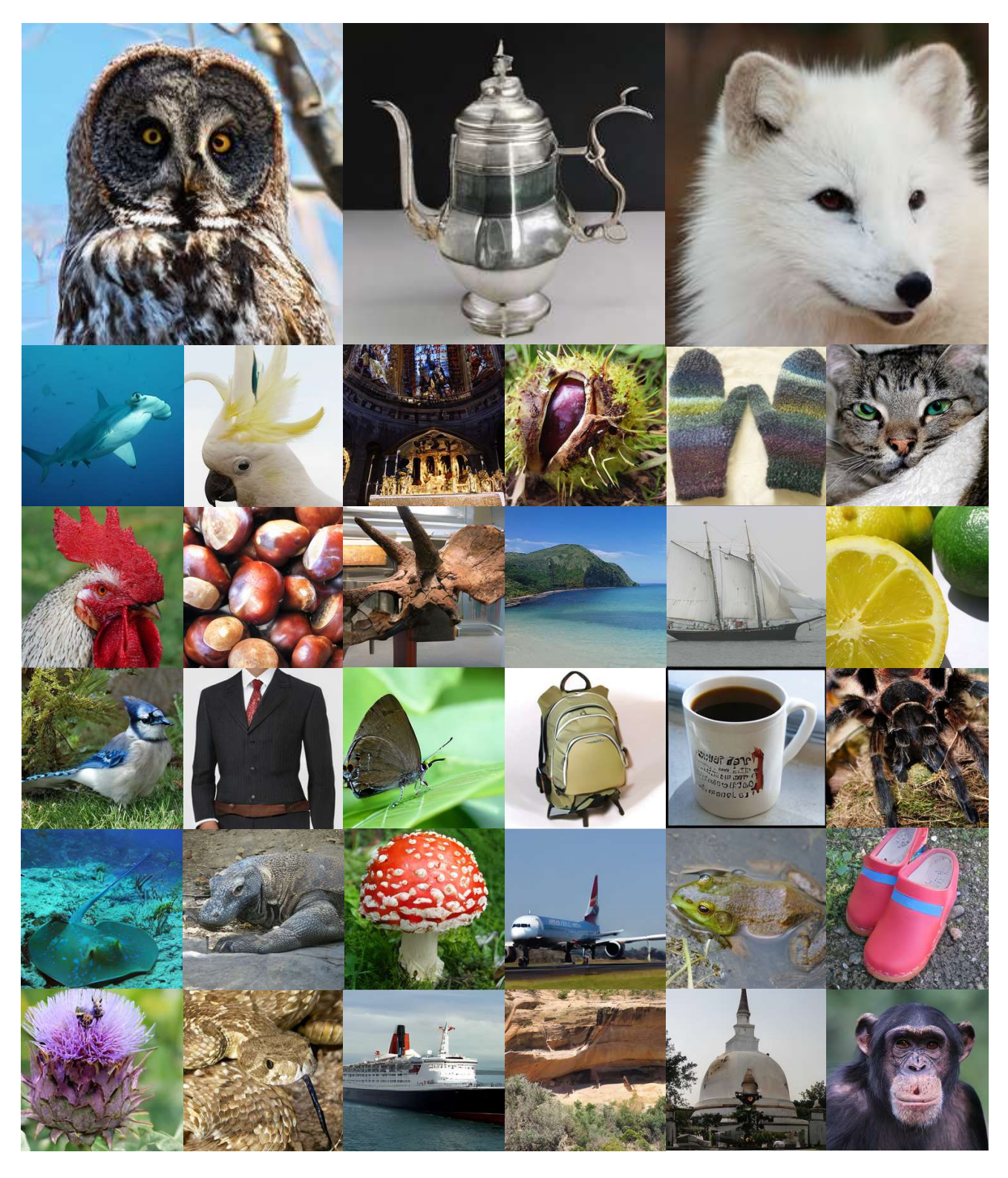


Figure 2. Qualitative results of MARVAL-RL-H.